ELSEVIER

Journal of Fluids and Structures 22 (2006) 919–928

JOURNAL OF FLUIDS AND STRUCTURES

www.elsevier.com/locate/jfs

Turbulent wake of a finite circular cylinder of small aspect ratio

M.S. Adaramola[a], O.G. Akinlade[b], D. Sumner[b,*], D.J. Bergstrom[b], A.J. Schenstead[b]

[a]*Division of Environmental Engineering, University of Saskatchewan, 57 Campus Drive, Saskatoon, Sask., Canada S7N 5A9*
[b]*Department of Mechanical Engineering, University of Saskatchewan, 57 Campus Drive, Saskatoon, Sask., Canada S7N 5A9*

Received 25 July 2005; accepted 15 April 2006
Available online 24 July 2006

Abstract

The turbulent wake of a finite circular cylinder mounted normal to a wall and partially immersed in a turbulent boundary layer was studied experimentally using two-component thermal anemometry in a low-speed wind tunnel. Four circular cylinders of aspect ratios AR = 9, 7, 5, and 3 were tested at a Reynolds number of $Re_D = 6 \times 10^4$. The cylinders were either completely or partially immersed in the wall boundary layer, where the boundary layer thickness relative to the cylinder diameter was $\delta/D = 3.0$. A similar turbulent wake structure (mean velocity, turbulence intensity, and Reynolds shear stress distributions) was found for cylinders of AR = 9, 7, and 5, while a distinctly different turbulent wake structure was found for the cylinder of AR = 3. This was consistent with the results of a previous study that focused on the time-averaged streamwise vortex structures in the wake.

1. Introduction

The turbulent wake of a two-dimensional or "infinite" circular cylinder of diameter D is characterized by the Kármán vortex street over a wide range of Reynolds number. For a circular cylinder of finite height H mounted normal to plane wall (Fig. 1), the wake is more complex and three-dimensional. The boundary layer flow around the base of the finite cylinder and the flow over the free end cause distinct changes in the flow pattern along the cylinder height, in particular the formation of a counter-rotating pair of tip vortices at the free end that extends in the streamwise direction into the wake (Kawamura et al., 1984; Park and Lee, 2000, 2002, 2004; Sumner et al., 2004). The tip vortices interact in a complex manner with Kármán vortex shedding from the sides of the cylinder, and are responsible for a downward-directed local velocity field near the free end, referred to as "downwash." In addition to the tip vortex structures, a pair of weaker base vortex structures (distinct from the horseshoe vortex) may be found close to the cylinder–wall junction and within the boundary layer developed on the wall (Tanaka and Murata, 1999; Sumner et al., 2004).

The flow field of the finite cylinder and the interactions between the tip vortices, base vortices, and Kármán vortex shedding, are strongly influenced by the cylinder's aspect ratio, $AR = H/D$, and the thickness of the boundary layer, δ, developed on the wall relative to the cylinder height and diameter, i.e. the ratios δ/H and δ/D (Fig. 1). For higher aspect

*Corresponding author. Tel.: +1 306 966 5537; fax: +1 306 966 5427.
E-mail address: david.sumner@usask.ca (D. Sumner).

0889-9746/$ - see front matter
doi:10.1016/j.jfluidstructs.2006.04.007

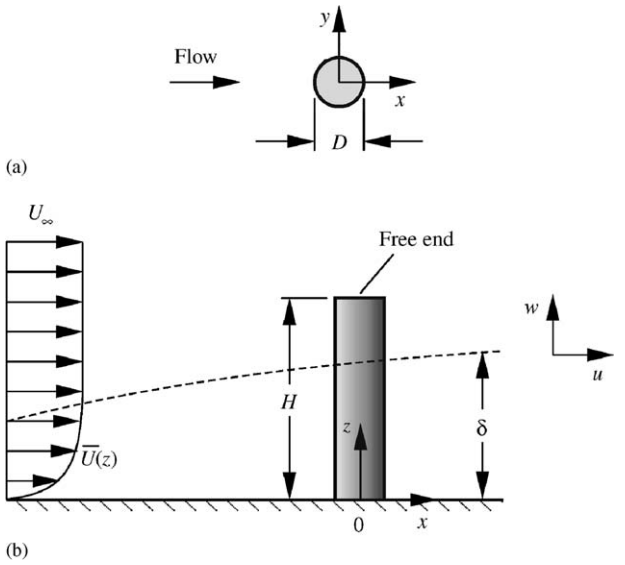

Fig. 1. Circular cylinder of finite height mounted normal to a ground plane and immersed in a boundary layer: (a) top view; (b) side view.

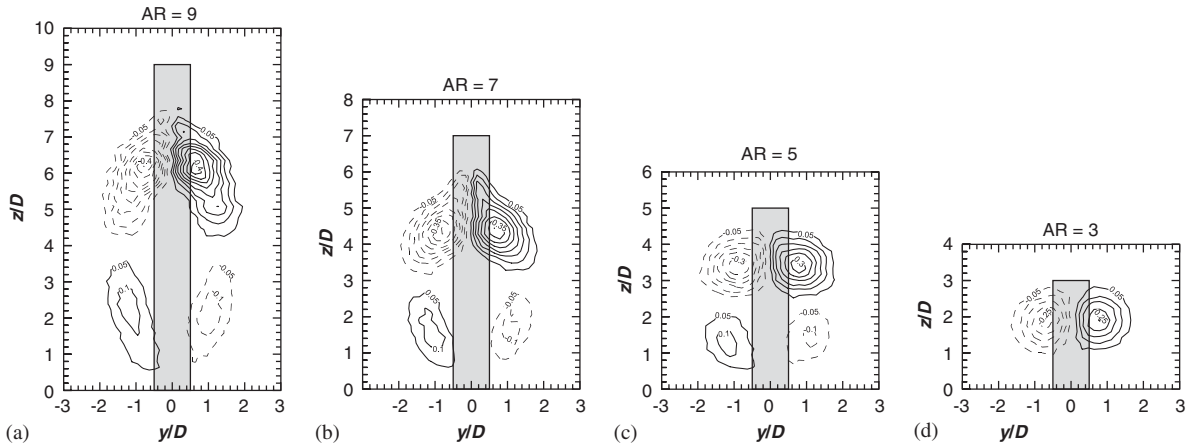

Fig. 2. Mean streamwise vorticity field from Sumner et al. (2004), $Re_D = 6 \times 10^4$, $\delta/D = 2.6$, $x/D = 6$: (a) AR = 9; (b) AR = 7; (c) AR = 5; (d) AR = 3. Contours of dimensionless vorticity, contour increment of 0.05, minimum vorticity contour ± 0.05, solid lines represent positive (CCW) vorticity, dashed lines represent negative (CW) vorticity.

ratios, the vortex shedding frequency (or Strouhal number, St) may vary in a cellular fashion along the cylinder height, each cell having a different frequency, with shedding being suppressed near the free end and near the cylinder–wall junction. The cellular structure disappears at lower aspect ratios, becoming a single cell of uniform St along the entire height for AR < 7 (Uematsu et al., 1990; Okamoto and Sunabashiri, 1992), particularly when δ/H is large (Sakamoto and Oiwake, 1984). For smaller aspect ratios, however, the flow around the free end may completely suppress antisymmetric Kármán vortex shedding from the cylinder, from the base to the tip. The critical aspect ratio below which antisymmetric vortex shedding is suppressed varies between the different studies in the literature, from AR = 1 to 7. The different critical values for AR are caused, in part, by the influence of the plane wall boundary layer (Luo, 1993), which differs in relative thickness (δ/D and δ/H) between the various studies. At and below the critical aspect ratio, antisymmetric Kármán vortex shedding may be replaced with symmetric arch vortex shedding at a definite frequency (Taniguchi et al., 1981; Sakamoto and Arie, 1983; Okamoto and Sunabashiri, 1992; Tanaka and Murata, 1999), and the longitudinal tip vortices may no longer form (Fox and West, 1993).

Further insight into the distinct wake structure for cylinders smaller than the critical aspect ratio was obtained in recent experiments by Sumner et al. (2004), where a seven-hole pressure probe was used to examine the wake structure of finite circular cylinders of small aspect ratio (AR = 9, 7, 5, and 3) under conditions where the cylinder was partially immersed in a turbulent boundary layer ($\delta/D = 2.6$). From measurements of the time-averaged wake velocity and streamwise vorticity fields, see Fig. 2, they found that the wake structure of a very short circular cylinder of AR = 3 (Fig. 2(d)) was distinctly different from that of the more slender circular cylinders of AR = 9, 7, and 5 (Fig. 2(a)–(c)). For the latter case, when AR = 9, 7, or 5, the wake was characterized by a strong downwash flow from the free end, an upwash flow from base of the cylinder, a counter-rotating pair of tip vortex structures near the free end, and a second pair of counter-rotating vortices, known as base vortex structures, within the wall boundary layer; see Fig. 2(a)–(c). A strong Kármán vortex-shedding signal was found along most of the cylinder height. The streamwise vortex structures weakened with increasing streamwise distance from the cylinder. For AR = 3, which had a distinct wake structure, the tip vortices and downwash remained, but the base vortices and upwash were absent; see Fig. 2(d). Furthermore, the downwash extended almost to the wall and a strong vortex shedding signal was mostly absent along the cylinder height, except in the region close to the wall, where a weak signal was detected.

Despite the practical significance of this flow, the three-dimensional separated flow field of a finite cylinder remains much less well understood than the classical case of the "infinite" cylinder, and there have been relatively few measurements of the turbulent wake of small-aspect-ratio circular cylinders reported in the literature. Two studies that have extensively measured the wake of the finite cylinder, by Tanaka and Murata (1999) and Sumner et al. (2004), provided no information on the fluctuating velocity field, which is important for understanding the transport properties of the wake. Okamoto and Sunabashiri (1992) measured the three turbulence intensity components in the wakes of finite circular cylinders of AR = 1–7, but the measurements were restricted to profiles at mid-height ($z/H = 0.5$, where z is the wall-normal coordinate direction). Leder (2003) measured the time-averaged streamwise vorticity field and the turbulent kinetic energy distribution in the wake of a short circular cylinder of AR = 2 using three-component LDV, but the measurements were mostly restricted to the recirculation zone close to the cylinder ($x/D < 3.6$, where x is the streamwise coordinate direction measured from the centre of the cylinder). The PIV measurements of Park and Lee (2004) provided some information on the turbulent velocity field, but were focused on the free end and recirculation zone regions.

The flow around the finite cylinder is sufficiently complex that further study is needed to better understand the flow field. The present study was therefore initiated to improve the understanding of the turbulent wake of finite circular cylinders of small aspect ratio.

2. Experimental set-up and instrumentation

The set-up for the finite-cylinder experiment (Fig. 3) was similar to that adopted by Sumner et al. (2004). The experiments were performed in a low-speed, closed-return wind tunnel with a test-section of 0.91 m (height) × 1.13 m (width) × 1.96 m (length). The longitudinal freestream turbulence intensity was less than 0.5%. A ground plane was installed on the floor of the wind tunnel test section. A rough strip near the leading edge of the ground plane was used to

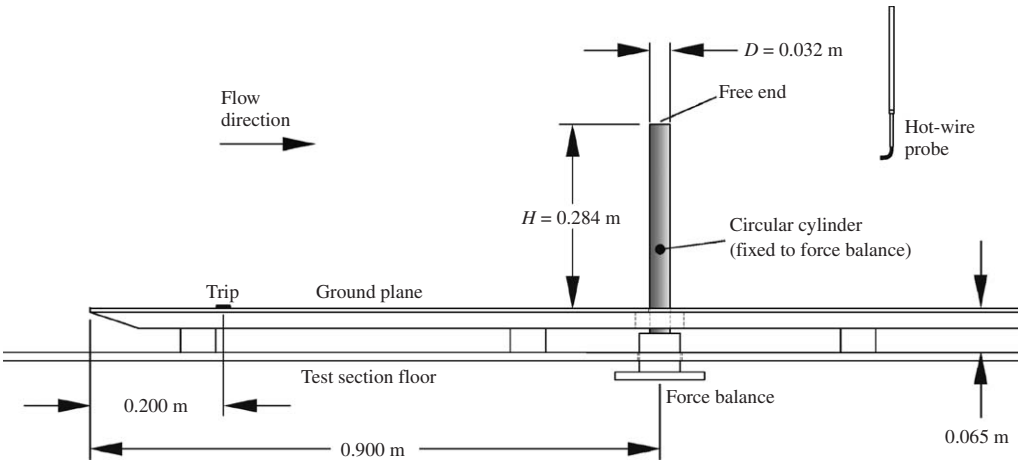

Fig. 3. Experimental set-up in the wind tunnel (cylinder with AR = 9 shown).

produce a fully developed turbulent boundary layer at the location of the cylinder. A three-axis, computer-controlled probe traversing system was used for the wake measurements.

2.1. Experimental apparatus

Four different, smooth, aluminium circular cylinder models, all of the same diameter, $D = 31.5$ mm, were tested. The free end of each cylinder was a flat surface with sharp edge. Each cylinder had a different height, giving cylinders with AR = 9, 7, 5, and 3, similar to the experiments of Sumner et al. (2004).

The cylinder model being tested was mounted to a six-component force balance below the test section at a distance of 900 mm from the entrance (and 700 mm from the rough strip on the ground plane); see Fig. 3. The cylinder extended vertically into the test section through a hole in the ground plane, with a circumferential gap of about 1 mm around the cylinder, and was partially immersed in the turbulent boundary layer on the ground plane. The solid blockage ratio was at most 0.9% and no wall interference corrections were made. The experiments were conducted at a freestream velocity of $U_\infty = 30$ m/s, giving a Reynolds number, based on cylinder diameter, of $\mathrm{Re}_D = 6 \times 10^4$.

2.2. Measurement instrumentation

The wind-tunnel data were acquired using a computer with a 1.8-GHz Intel Pentium 4 processor, a National Instruments PCI-6031E 16-bit data acquisition board, and LabVIEW software. The freestream conditions were obtained with a Pitot-static probe and Datametrics Barocell absolute and differential pressure transducers.

The velocity profile in the boundary layer on the ground plane was measured with a TSI model 1243-20 constant-temperature boundary-layer cross-film probe and a TSI IFA-100 anemometer. The probe was oriented to measure the streamwise, u, and wall-normal, w, velocity components (the directions of the velocity components are shown in Fig. 1). At the location of the cylinder (with the cylinder removed), the boundary layer thickness was $\delta = 95$ mm, the boundary layer shape factor was $H = 1.3$, and the Reynolds number based on momentum thickness, θ, was $\mathrm{Re}_\theta = 1.7 \times 10^4$. This boundary layer provided a thickness-to-diameter ratio of $\delta/D = 3.0$ and a thickness-to-height ratio ranging from partially immersed, $\delta/H = 0.3$ (for AR = 9), to fully immersed, $\delta/H = 1.0$ (for AR = 3).

Wake velocity measurements were made with the same boundary layer cross-film probe. The probe had the same orientation as the boundary layer measurements, to measure the streamwise, u, and wall-normal, w, velocity components in the cylinder wake. At each measurement point, 100 000 instantaneous velocity data per channel were acquired at a sampling rate of 10 kHz per channel after low-pass filtering at 5 kHz. The uncertainties in the streamwise and wall-normal fluctuating velocity components were estimated as $\pm 4\%$ and $\pm 7\%$, respectively, while the uncertainty in the Reynolds shear stress was estimated to be $\pm 9\%$.

For each cylinder, the wake velocity field in the cross-stream (y–z) plane was measured over a 5 mm uniform grid at streamwise locations of $x/D = 6$ and 10 downstream of the cylinder, corresponding to two of the streamwise locations measured by Sumner et al. (2004). The measurement plane extended in the cross-stream direction to $y = \pm 80$ mm, and in the wall-normal direction from $z = 5$ to 300 mm (for the cylinder of AR = 9). No measurements were made for $x/D < 6$ because of the high flow angles encountered in the downwash flow field close to the free end (Sumner et al., 2004).

3. Results and discussion

3.1. Mean velocity distribution

Time-averaged streamwise velocity fields ($\overline{U}/U_\infty$) in the cross-stream (y–z) plane at $x/D = 6$ are shown in Fig. 4. The lateral (y-direction) spread of the wake with streamwise distance from the cylinder is evident, with the tendency to spread reducing as AR increases (and the flow around the cylinder becomes more two-dimensional). For AR = 9, 7, and 5 (Fig. 4(a)–(c)), the streamwise velocity field is similar, with the lowest mean streamwise velocities found in a concentrated region behind the cylinder well above the ground plane (and close to the mid-height position, $z/H = 0.5$). With increasing x/D, the centre of this region descends towards the base of the cylinder and the velocity defect reduces. Compared to Fig. 2(a)–(c), it is seen that this region of low streamwise velocity is bounded on the four corners by the tip and base vortex structures. For AR = 3, the lowest streamwise velocities occur very close to the ground plane immediately behind the cylinder, and the concentrated region of low velocity near mid-height is absent (Fig. 4(d)), as are the base vortex structures (Fig. 2(d)). This result shows the distinct wake structure for this cylinder and indicates that the critical aspect ratio in these experiments lies between AR = 3 and 5.

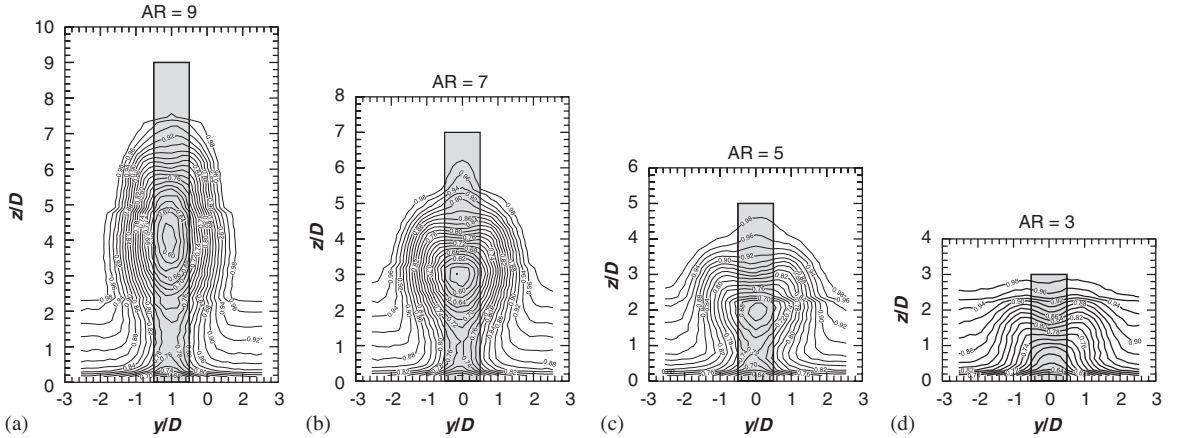

Fig. 4. Streamwise mean velocity field in the wake of the circular cylinder, $\delta/D = 3.0$, $x/D = 6$: (a) AR = 9; (b) AR = 7; (c) AR = 5; (d) AR = 3. Contours of $\overline{U}/U_\infty$, contour increment of 0.02.

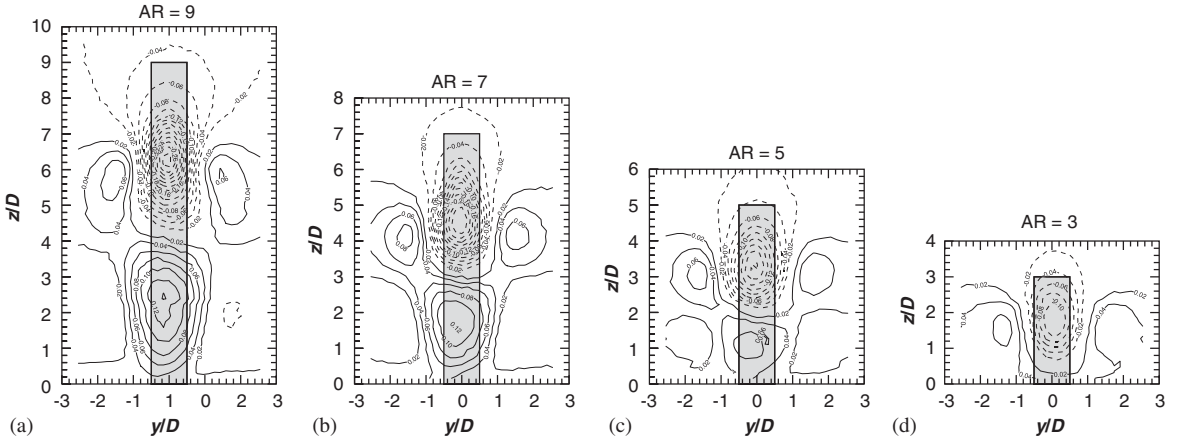

Fig. 5. Wall-normal mean velocity field in the wake of the circular cylinder, $\delta/D = 3.0$: (a) AR = 9; (b) AR = 7; (c) AR = 5; (d) AR = 3. Contours of $\overline{W}/U_\infty$, contour increment of 0.02. Solid lines represent positive (upwards) velocity, dashed lines represent negative (downwards) velocity.

Time-averaged wall-normal velocity fields ($\overline{W}/U_\infty$) in the cross-stream (y–z) plane at $x/D = 6$ are shown in Fig. 5. The presence of a strong downwash velocity (shown by the dashed contour lines in Fig. 5) originating near the free end is observed for all four aspect ratios. The downwash is located between, and induced by, the prominent tip vortex structures (Fig. 2). The strength of the downwash velocity field increases with AR but decreases with x/D. For AR = 9, 7, and 5 (Fig. 5(a)–(c)), there is an upwash velocity (shown by the solid contour lines in Fig. 5) originating near the base of the cylinder, the strength of which also increases with AR and decreases with x/D. The upwash is centred between, and induced by, the base vortex structures within the plane wall boundary layer (Fig. 2(a)–(c)). In the case of AR = 3 (Fig. 5(d)), downwash extends to the ground plane and upwash is absent. The absence of the upwash for AR = 3 coincides with the absence of the base vortex structures (Fig. 2(d)), and is another characteristic of the distinct wake structure for the shortest cylinder.

3.2. Mean streamwise velocity defect

Fig. 6(a) presents some cross-stream profiles of streamwise mean velocity defect at the mid-height of the cylinder ($z/H = 0.5$). The streamwise mean velocity defect for AR = 3 at $x/D = 6$ has two peaks while those for AR = 9, 7, and 5 have a single peak. The appearance of two peaks in some of the velocity defect profiles is caused by the effect of

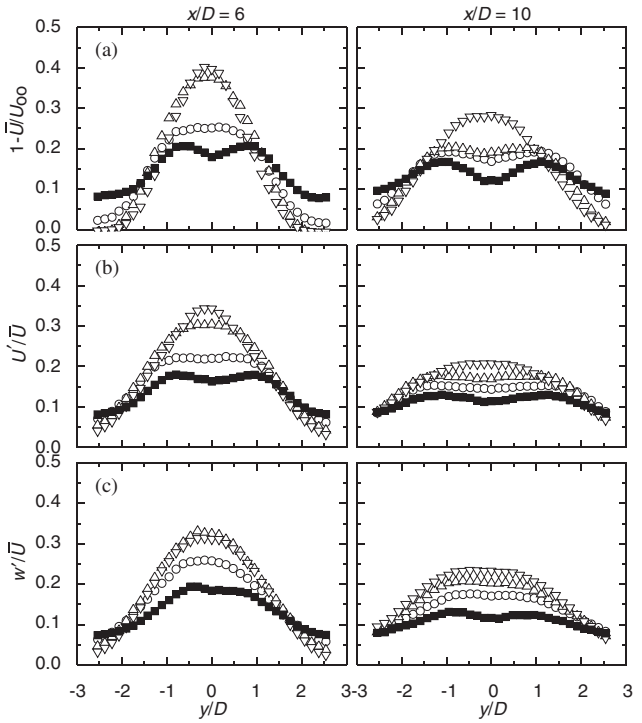

Fig. 6. Wake profiles at mid-height ($z/H = 0.5$): (a) mean streamwise velocity defect; (b) streamwise turbulence intensity; (c) wall-normal turbulence intensity. ■, AR = 3 ($\delta/H = 1.0$); ○, AR = 5 ($\delta/H = 0.6$); △, AR = 7 ($\delta/H = 0.4$); ▽, AR = 9 ($\delta/H = 0.3$).

downwash from the free end (Okamoto and Sunabashiri, 1992). The value of velocity at the midpoint (on the wake centreline, at $y/D = 0$) between the two peaks indicates the excess velocity due to the downwash. For the distinct wake of AR = 3, downwash extends to the ground plane (Fig. 5(d)) and therefore two peaks are observed in the mean streamwise velocity defect profiles at both $x/D = 6$ and 10 (Fig. 6(a)). For the more slender cylinders of AR = 9, 7, and 5, downwash does not reach the centre section ($z/H = 0.5$) at $x/D = 6$, and the mean streamwise velocity defect profiles have only a single peak (Fig. 6(a)). This is similar to the results of Park and Lee (2002) for a cylinder of AR = 6 at $x/D = 5$, where only a single peak was observed in the mean streamwise velocity defect profile at mid-height. At $x/D = 10$, however, the vortex structures have descended toward the ground plane, downwash reaches the mid-height position for AR = 7 and 5, and there are now two peaks in the mean streamwise velocity defect (Fig. 6(a)).

The reason for these differences in the defect profiles (Fig. 6(a)) is also related to the boundary layer thickness (δ/H) relative to the mid-height of the cylinder ($z/H = 0.5$). For the tallest cylinder of AR = 9, the boundary layer thickness remains less than mid-height ($z/H = 0.5$) at $x/D = 0$ ($\delta/H = 0.3$), $x/D = 6$ ($\delta/H = 0.38$), and $x/D = 10$ ($\delta/H = 0.40$), leading to the single-peak velocity defect profile at both $x/D = 6$ and 10 (Fig. 6(a)). For the shortest cylinder of AR = 3, the cylinder is completely immersed in the boundary layer at $x/D = 0$ ($\delta/H = 1.0$), and the two-peak velocity defect profile is seen at both $x/D = 6$ ($\delta/H = 1.1$) and $x/D = 10$ ($\delta/H = 1.2$) (Fig. 6(a)). For the intermediate aspect ratios, AR = 7 and 5, where $\delta/H = 0.4$ and 0.6 at the location of the cylinder ($x/D = 0$), respectively, the shape of the defect profile changes from the single-peak shape to the two-peak shape when moving from $x/D = 6$ to $x/D = 10$ (Fig. 6(a)).

The velocity defect data also show that the cylinder with AR = 3 has a much wider wake at $z/H = 0.5$ than the cylinders of AR = 5, 7, and 9, with appreciable velocity defect at $y/D = \pm 3.0$. For all cylinders, the maximum velocity defect reduces with distance from the cylinder.

3.3. Turbulence intensities

Profiles of the streamwise turbulent intensity $\left(u'/\overline{U}\right)$ and wall-normal turbulence intensity $\left(w'/\overline{U}\right)$ at mid-height ($z/H = 0.5$) are given in Fig. 6(b) and (c), respectively. There is an overall reduction in turbulence intensity at this

vertical position, and a gradual change from single-peak behaviour to double-peak behaviour, with increasing x/D. The wall-normal turbulence intensities (Fig. 6(c)) are slightly higher than the streamwise turbulence intensities (Fig. 6(b)). The data show the distinctly different wake structure for AR = 3, which has the lowest levels of turbulence intensity at mid-height and the widest lateral wake spread of the four aspect ratios tested. The profiles nearly collapse for AR = 9 and 7, however, the profiles for AR = 5 are distinct, suggesting that a transitional wake structure may exist between the shortest (AR = 3) and tallest (AR = 7 and 9) cylinders (although this is based only on measurements at mid-height).

Distributions of $u'/\overline{U}$ and $w'/\overline{U}$ in the cross-stream plane, shown in Figs. 7 and 8, respectively, are similar in many respects to the mean streamwise velocity fields (Figs. 4 and 5). For AR = 9, 7, and 5, localized regions of high streamwise (Fig. 7(a)–(c)) and wall-normal turbulence intensity (Fig. 8(a)–(c)) behind the cylinder coincide with the regions of low streamwise mean velocity (Fig. 4(a)–(c)) bounded on the four corners by the tip and base vortices (Fig. 2(a)–(c)). This region of high $u'/\overline{U}$ and $w'/\overline{U}$ is caused by the interactions between the vortex structures, the vortex street, downwash from the free end, and upwash from the ground plane that produces strong shear. In the case of AR = 3, the localized region of high $u'/\overline{U}$ disappears (Fig. 7(d)) because the base vortex structures (Fig. 2(d)) and upwash (Fig. 5(d)) are absent. However, a localized region of high $w'/\overline{U}$ is still detected close to the ground plane (Fig. 8(d)). For all four cylinders, the peak levels of turbulence intensity reduce with x/D, and the downwash causes them to move closer to the ground plane.

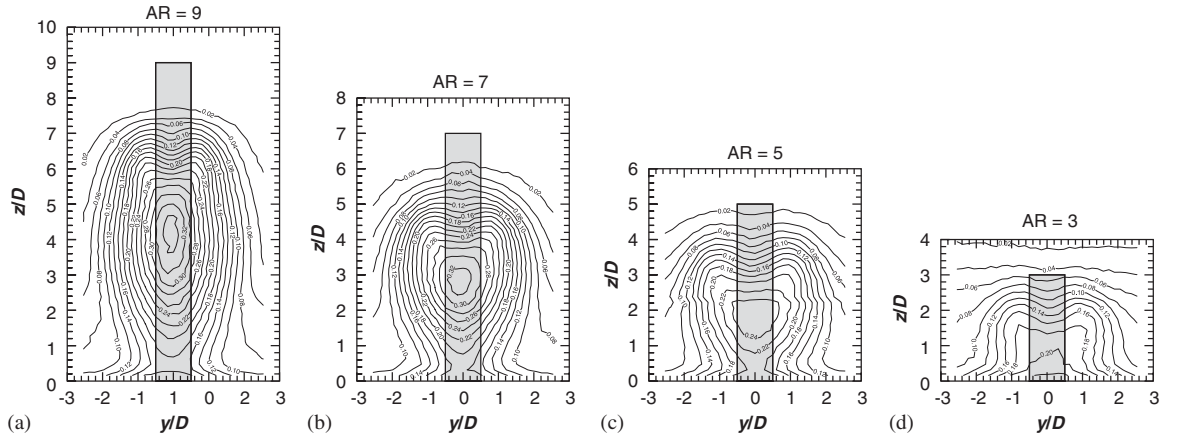

Fig. 7. Streamwise turbulence intensity field in the wake of the circular cylinder, $\delta/D = 3.0$, $x/D = 6$: (a) AR = 9; (b) AR = 7; (c) AR = 5; (d) AR = 3. Contours of $u'/\overline{U}$, contour increment of 0.02.

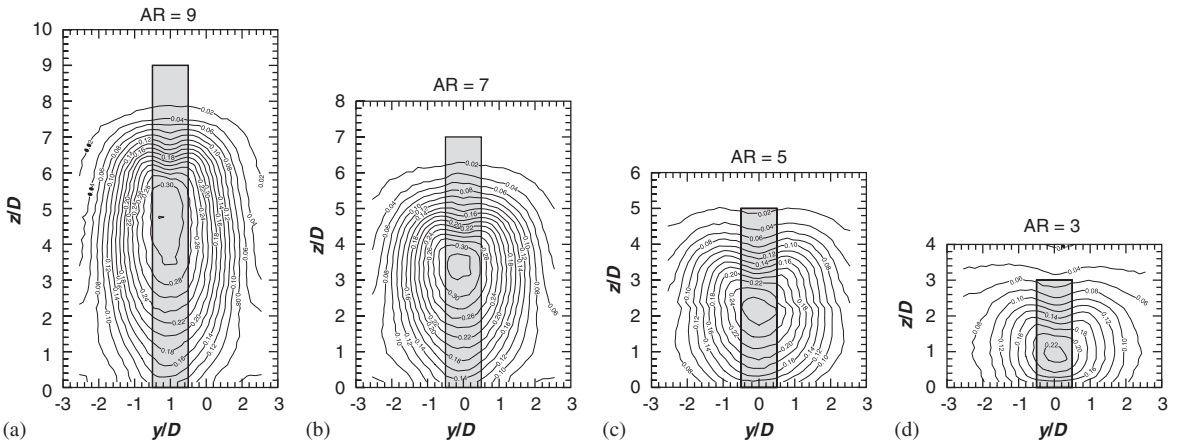

Fig. 8. Wall-normal turbulence intensity field in the wake of the circular cylinder, $\delta/D = 3.0$, $x/D = 6$: (a) AR = 9; (b) AR = 7; (c) AR = 5; (d) AR = 3. Contours of $w'/\overline{U}$, contour increment of 0.02.

Fig. 9(a) and (b) show the streamwise and wall-normal turbulence intensity distributions, respectively, along the wake centreline ($y/D = 0$) for all four cylinders at $x/D = 6$. Since the tip vortex and base vortex strengths increase with AR (Sumner et al., 2004), there is a resultant overall increase in turbulence intensity with AR, due to the interactions between the streamwise vortices. The vortex structures, downwash and upwash weaken with increasing x/D (Sumner et al., 2004), and the result is a decrease in turbulence intensity with x/D. There is also a reduction in turbulence intensity towards the free end similar to what was observed by Park and Lee (2000) for a cylinder with AR = 10.

A distinctly different turbulent wake structure is observed for AR = 3, which has the lowest overall levels of turbulence intensity, the largest wake spread in the wall-normal direction at a given x/D, and an absence of a peak streamwise turbulence intensity near mid-height (Fig. 9(a)). The larger vertical extent of the wake occurs for AR = 3 because the tip vortices occur closer to the free end than for AR = 9, 7, and 5 (Sumner et al., 2004). The shapes of the turbulence intensity profiles for AR = 3 are also similar to that of the plane wall boundary layer (not shown), although with higher magnitudes. Similar to the cross-stream profiles at mid-height shown in Fig. 6(b) and (c), the turbulence intensity data on the wake centreline for AR = 9 and 7 (Fig. 9(a) and (b)) nearly collapse onto a single curve, but the data for AR = 5 suggest a transitional turbulent wake structure between the shortest (AR = 3) and longest (AR = 9 and 7) cylinders.

3.4. Reynolds shear stress

The streamwise development of the Reynolds shear stress distribution $\left(-\overline{u'w'}/\overline{U}^2\right)$ on the wake centreline ($y/D = 0$) is shown in Fig. 9(c). Its behaviour is similar for AR = 9, 7, and 5, with two regions of elevated Reynolds shear stress, each of opposite sign. The Reynolds shear stress profiles for AR = 3 are distinct (Fig. 9(c)), where the absence of the base vortex structures and upwash coincides with the vanishing of negative shear stress. These profiles are similar in some respects to that of the plane wall boundary layer (not shown), although they are larger in magnitude. The Reynolds shear stress profile for AR = 5 at $x/D = 10$ suggests that a transitional turbulent wake structure may exist for this cylinder.

The Reynolds shear stress distribution in the cross-stream (y–z) plane is shown in Fig. 10. Its behaviour is similar for AR = 9, 7, and 5 (Fig. 10(a)–(c)), with two regions of elevated Reynolds shear stress, each of opposite sign, located behind the cylinder. The region of positive Reynolds shear stress is located in the region of downwash flow from the free end and centred between the tip vortex structures (Fig. 2(a)–(c)). The region of negative Reynolds shear stress occurs within the plane wall boundary layer in the region of the upwash flow, and is centred between the base vortex structures (Fig. 2(a)–(c)). The boundary between these two regions approximately coincides with the regions of lowest streamwise mean velocity (Fig. 4(a)–(c)) and highest turbulence intensity (Figs. 7(a)–(c), 8(a)–(c)), and is centred in the midst of the four vortex structures and where the downwash and upwash flows interact (Fig. 5(a)–(c)). The Reynolds shear stress distribution for AR = 3 is distinct (Fig. 10(d)), where the absence of upwash from the ground plane and the base vortex structures (Fig. 2(d)) means an absence of any negative Reynolds shear stress.

For all cylinders, the peak absolute values of Reynolds shear stress decrease with x/D. The peak absolute value of Reynolds shear stress increases with AR (Figs. 9(c), 10) as do the strengths of the streamwise vortex structures and the downwash and upwash velocity fields (Sumner et al., 2004).

4. Conclusions

In the present study, the turbulent wake structure of a finite circular cylinder mounted normal to a ground plane was investigated using two-component thermal anemometry in a low-speed wind tunnel. The probe was oriented to measure the streamwise and wall-normal velocity components, and the mean velocity, turbulence intensity, and Reynolds shear stress fields were obtained. Four circular cylinders, with AR = 9, 7, 5, and 3, were used for the experiments, which were conducted in the subcritical Reynolds number regime, $\mathrm{Re}_D = 6 \times 10^4$. The cylinders were either completely or partially immersed in a turbulent flat-plate boundary layer, which had a thickness of $\delta/D = 3.0$ at the location of the cylinder.

The results of this study have improved the current state of information on the wake of a finite circular cylinder, which is limited. For example, the time-averaged streamwise vorticity field and the turbulent kinetic energy distribution in a finite-cylinder wake were determined by Leder (2003), but the results were mostly restricted to the recirculation zone, and were made only for one cylinder aspect ratio, of AR = 2. The wake studies of Tanaka and Murata (1999) and Sumner et al. (2004), while comprehensive, were limited to mean velocity and vorticity measurements. Okamoto and Sunabashiri (1992) measured the three turbulence intensity components in the wake of a finite cylinder, but their measurements were restricted to profiles at the mid-height position only. More detailed measurements were made by

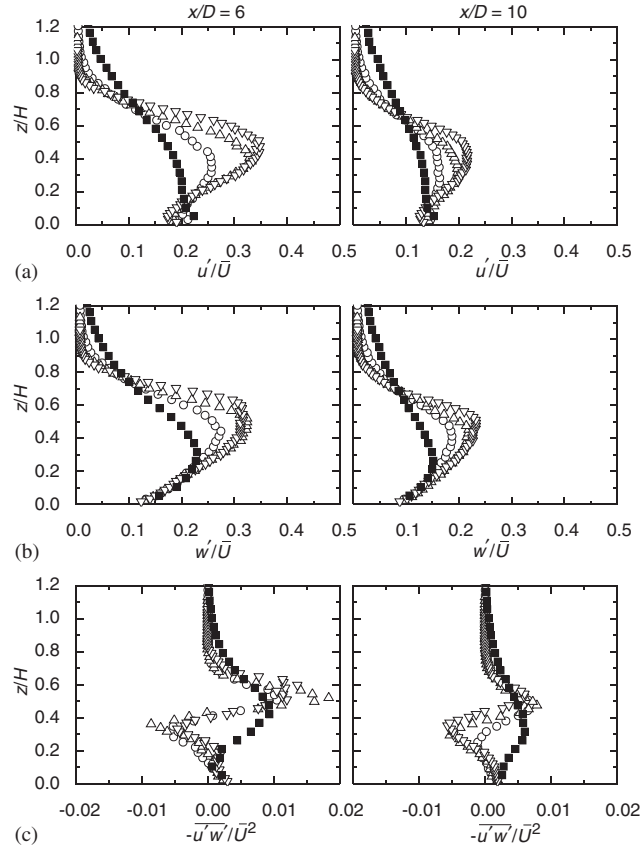

Fig. 9. Wake profiles along the wake centreline ($y/D = 0$): (a) streamwise turbulence intensity; (b) wall-normal turbulence intensity; (c) Reynolds shear stress. ■, AR = 3; ○, AR = 5; △, AR = 7; ▽, AR = 9.

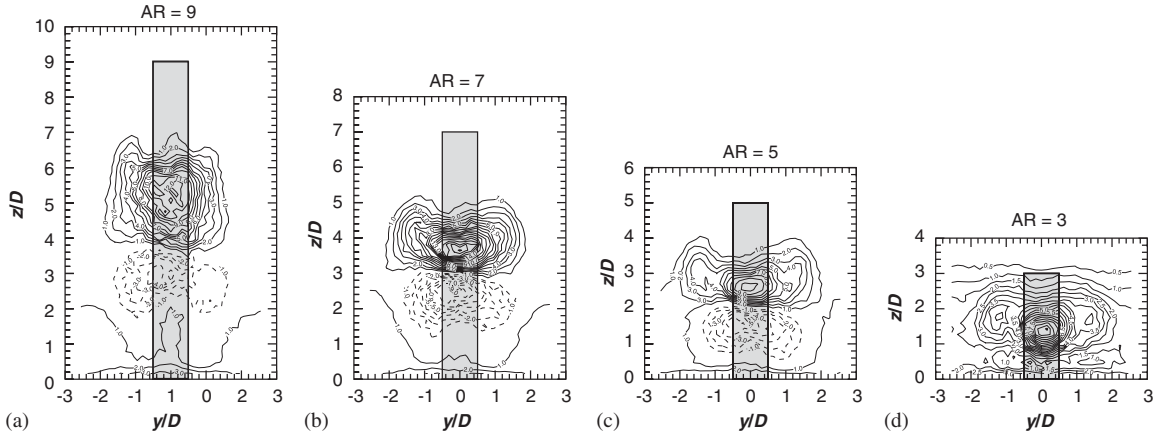

Fig. 10. Reynolds shear stress field in the wake of the circular cylinder, $\delta/D = 3.0$, $x/D = 6$: (a) AR = 9; (b) AR = 7; (c) AR = 5; (d) AR = 3. Contours of $-\overline{u'w'}/\overline{U}^2 \times 10^3$, contour increments of 0.5×10^3 (for AR = 3) or 1.0×10^3 (for AR = 9, 7, and 5).

Park and Lee (2004), who used PIV to study the turbulent velocity field near the free end and in the recirculation zone of a finite cylinder. However, their study focused mostly on the effects of free end shape and were made at only one cylinder aspect ratio, AR = 6.

In the present study, the cylinders of AR = 9, 7, and 5 had a similar turbulent wake structure, with a localized region of low streamwise mean velocity and high turbulence intensity behind the cylinder, which was centred between the four main streamwise vortex structures. A strong downwash velocity field was found between the tip vortex structures closer to the free end, and an upwash velocity field was found between the base vortex structures closer to the ground plane. The sign of the Reynolds shear stress changed near the mid-height of the cylinder between the two pairs of vortex structures, where the downwash and upwash flow fields meet.

The mean velocity, turbulence intensity, and Reynolds shear stress fields for the cylinder with AR = 3 indicate that this cylinder had a distinct turbulent wake structure. This result occurs because of the absence of the base vortex structures and their associated upwash velocity field from the ground plane. Some of the data suggest a transitional turbulent wake structure may exist for the cylinder with AR = 5.

Acknowledgments

The authors acknowledge the support of the Natural Sciences and Engineering Research Council (NSERC) of Canada, the Canada Foundation for Innovation (CFI), the Innovation and Science Fund of Saskatchewan, and the University of Saskatchewan USTEP program. The assistance of D. Deutscher and Engineering Shops is appreciated.

References

Fox, T.A., West, G.S., 1993. Fluid-induced loading of cantilevered circular cylinders in a low-turbulence uniform flow, Part 1: mean loading with aspect ratios in the range 4–30. Journal of Fluids and Structures 7, 1–14.

Kawamura, T., Hiwada, M., Hibino, T., Mabuchi, T., Kumada, M., 1984. Flow around a finite circular cylinder on a flat plate. Bulletin of the JSME 27, 2142–2150.

Leder, A., 2003. 3D-flow structures behind truncated circular cylinders. In: Proceedings of FEDSM'03, Fourth ASME–JSME Joint Fluids Engineering Conference, Honolulu, USA, Paper No. FEDSM2003-45083.

Luo, S.C., 1993. Flow past a finite length circular cylinder. In: Proceedings of the Third (1993) International Offshore and Polar Engineering Conference, Singapore, vol. III, ISOPE: Golden, CO, USA, pp. 530–534.

Okamoto, S., Sunabashiri, Y., 1992. Vortex shedding from a circular cylinder of finite length placed on a ground plane. ASME Journal of Fluids Engineering 144, 512–521.

Park, C.-W., Lee, S.-J., 2000. Free end effects on the near wake flow structure behind a finite circular cylinder. Journal of Wind Engineering and Industrial Aerodynamics 88, 231–246.

Park, C.-W., Lee, S.-J., 2002. Flow structure around a finite circular cylinder embedded in various atmospheric boundary layers. Fluid Dynamics Research 30, 197–215.

Park, C.-W., Lee, S.-J., 2004. Effects of free-end corner shape on flow structure around a finite cylinder. Journal of Fluids and Structures 19, 141–158.

Sakamoto, H., Arie, M., 1983. Vortex shedding from a rectangular prism and a circular cylinder placed vertically in a turbulent boundary layer. Journal of Fluid Mechanics 126, 147–165.

Sakamoto, H., Oiwake, S., 1984. Fluctuating forces on a rectangular prism and a circular cylinder placed vertically in a turbulent boundary layer. ASME Journal of Fluids Engineering 106, 160–166.

Sumner, D., Heseltine, J.L., Dansereau, O.J.P., 2004. Wake structure of a finite circular cylinder of small aspect ratio. Experiments in Fluids 37, 720–730.

Tanaka, S., Murata, S., 1999. An investigation of the wake structure and aerodynamic characteristics of a finite circular cylinder. JSME International Journal Series B: Fluids and Thermal Engineering 42, 178–187.

Taniguchi, S., Sakamoto, H., Arie, M., 1981. Flow around circular cylinders of finite height placed vertically in turbulent boundary layers. Bulletin of the JSME 24, 37–44.

Uematsu, Y., Yamada, M., Ishii, K., 1990. Some effects of free-stream turbulence on the flow past a cantilevered circular cylinder. Journal of Wind Engineering and Industrial Aerodynamics 33, 43–52.